บทที่ 3 ผลการวิจัยและวิจารณ์

3.1. Site-directed mutagenesis of OsBADH1 and OsBADH2

This section describes the construction of OsBADH1 and OsBADH2 mutants by site-directed mutagenesis. The amino acids, either N164 and W172 of OsBADH1 or N162 and W170 of OsBADH2 were mutated to Alanine (A). Additionally, W172 and W170 of OsBADH1 and OsBADH2, respectively were mutated to Phenylalanine (F). The plasmids containing the desired mutation were transformed into *E. coli* strain XL-10 Gold and the transformant colonies were selected by kanamycin. The colony contained the mutated plasmid were verified by restriction enzyme analysis, colony PCR screening and DNA sequencing.

3.1.1 Construction of OsBADH1 and OsBADH2 mutants

Site-directed mutagenesis was carried out using pET28b-OsBADH1 and pET28b-OsBADH2 containing OsBADH1 and OsBADH2 as a template. The sense and antisense mutagenic primers are shown in Table 11 in methodology section. The mutants were N164A, W172A and W172F of OsBADH1 and N162A, W170A and W170F of OsBADH2. After PCR amplification, the parental DNA template was cut by *Dpn*I. The *Dpn*I endonuclease (target sequence: 5′-Gm6ATC-3′) specific for methylated and hemimethylated DNA was used to digest the parental DNA template and to select for plasmid containing mutated sequence. The PCR products of mutants were ran on 0.8% agarose gel electrophoresis and transformed into *E. coli*. The size of PCR product was about 6.8 kb and 7.1 kb for OsBADH1 and OsBADH2 mutants, respectively (Figure 3).

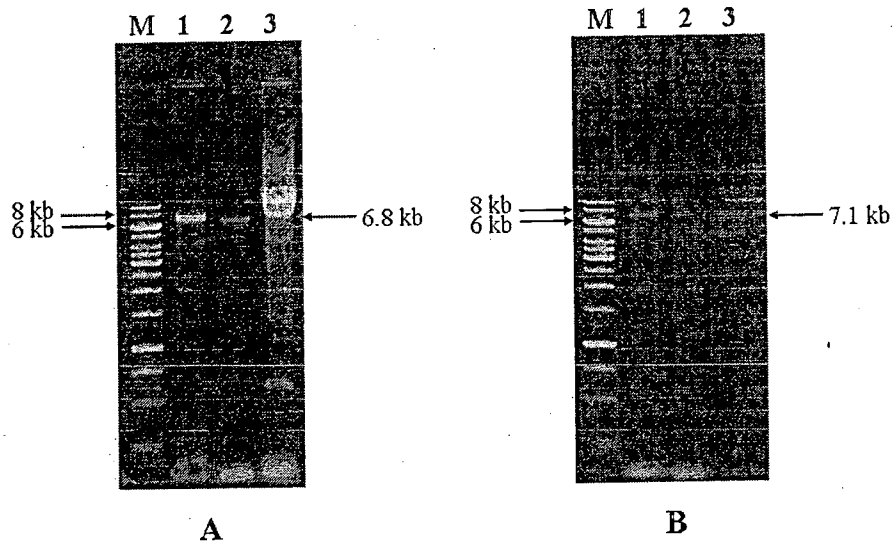

Figure 3 PCR product obtained from site-directed mutagenesis. (A) PCR amplification of OsBADH1 mutants; Lane M, GeneRuler DNA Ladder; Lane 1, PCR product of N164A; Lane 2, PCR product of W172A; Lane 3, PCR product of W172F; (B) PCR amplification of OsBADH2 mutants; Lane 1, PCR product of N162A; Lane 2, PCR product of W170A; Lane 3, PCR product of W170F.

3.1.2. PCR screening of OsBADH1 and OsBADH2 mutants

PCR screening was firstly used to check the presence of the mutants prior to DNA sequencing. To confirm mutated plasmid, the screening primers specific for mutated sequence were designed as shown in Table 3 in methodology section. The mutated plasmid containing the desired mutation ought to be amplified using the designed primers while non-mutated plasmids could not be amplified. The PCR screening products of either OsBADH1 or OsBADH2 mutants were checked by 0.8% agarose gel electrophoresis as shown in Figure 34 and Figure 35, respectively. The strong band of 1008 bp could be seen in N164A and N162A whereas the band of 948 bp could be seen in W172A, W172F, W170A and W170F. This indicated that all mutated plasmids contained the expected mutation. The colony containing the mutated plasmids were subsequently extracted and digested with *Xho*I and *Nde*I.

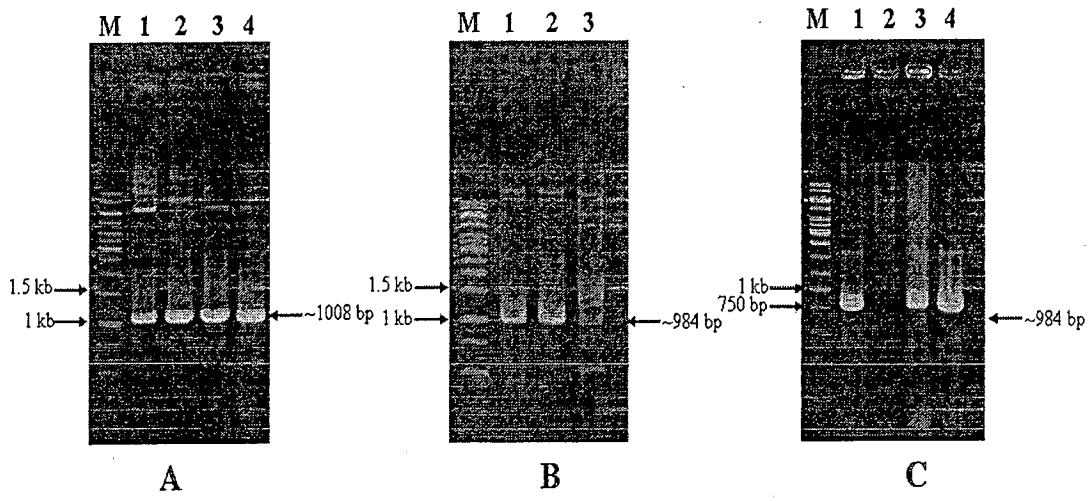

Figure 4 PCR screening of OsBADH1 mutants. (A) PCR screening of N164A; Lane M, GeneRuler DNA Ladder; Lane 1-4, PCR screening of N164A clone 1-4; (B) PCR screening of W172A; Lane 1-3, PCR screening of W172A clone 1-3; (C) PCR screening of W172F; Lane 1-4, PCR screening of W172F clone 1-4.

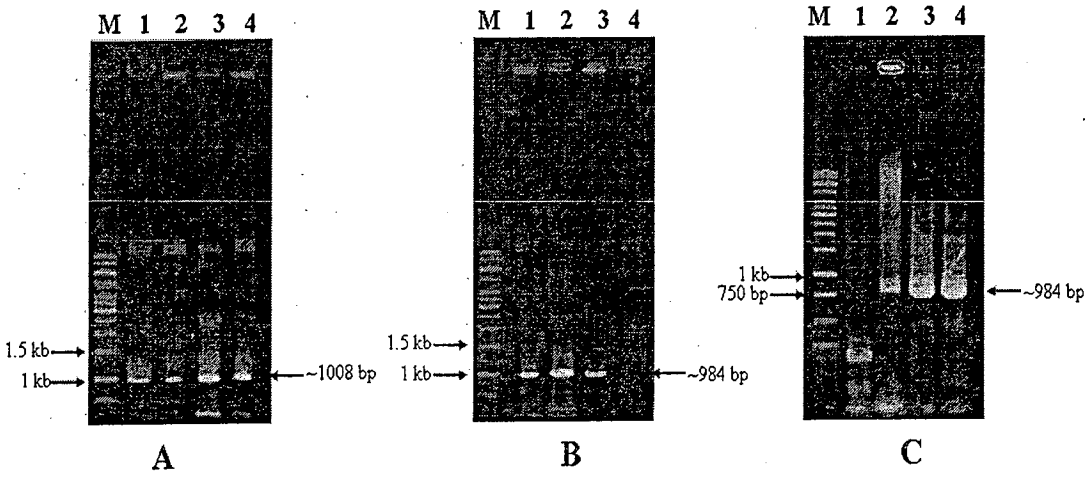

Figure 5 PCR screening of OsBADH2 mutants. (A) PCR screening of N162A; Lane M, GeneRuler DNA Ladder; Lane 1-4, PCR screening of N162A clone 1-4; (B) PCR screening of W170A; Lane 1-4, PCR screening of W170A clone 1-4; (C) PCR screening of W170F; Lane 1-4, PCR screening of W170F clone 1-4.

3.1.3. Restriction enzyme analysis of OsBADH1 and OsBADH2 mutants

To confirm whether the mutated plasmids contained the correct size of *OsBADH1* and *OsBADH2*, the restriction enzyme digestion with *Xho*I and *Nde*I of the chosen mutated plasmids were carried out. The digestion of the mutated plasmids generated two bands at 5.3 kb (represented size of plasmid pET28b) and 1.5 kb (represented size of *OsBADH1*) or 1.8 kb (represented size of *OsBADH2*) as shown in Figure 6 and Figure 7, respectively. In lane 2 of Figure 6A, the mutated plasmid was incompletely digested by *Xho*I and *Nde*I therefore giving the band of linearized pET28b-OsBADH1 above pET28b plasmid. In order to confirm the correction of the mutated gene, the mutated plasmids were sequenced. The sequence alignment of either OsBADH1 or OsBADH2 wide-type and mutants is shown in Figure 8 and Figure 9, respectively.

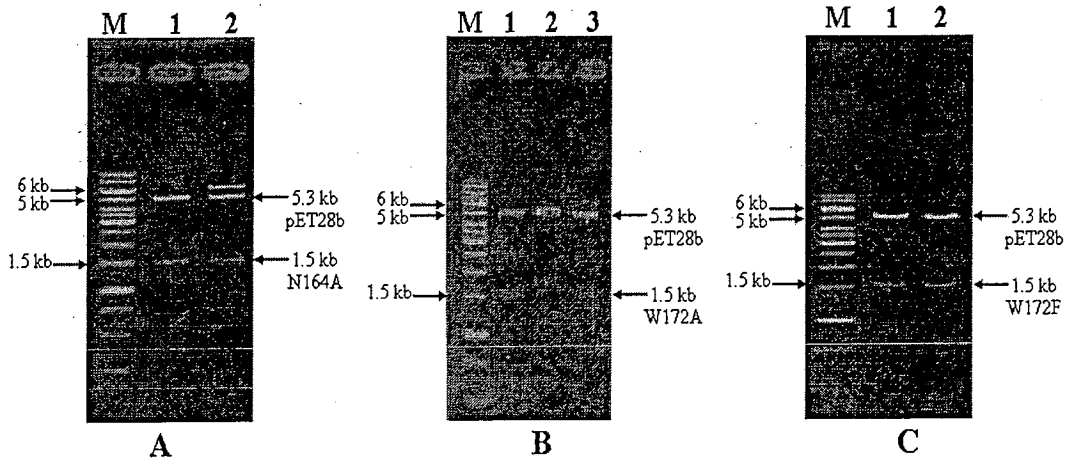

Figure 6 Restriction enzyme analysis of OsBADH1 mutants. (A) Restriction enzyme analysis of pET28b-N164A plasmids; Lane M, GeneRuler DNA Ladder; Lane 1 and 2, pET28b-N164A clone 1 and 2 digested with *Xho*I and *Nde*I; (B) Restriction enzyme analysis of pET28b-W172A plasmids; Lane 1-3, pET28b-W172A clone 1-3 digested with *Xho*I and *Nde*I; (C) Restriction enzyme analysis of pET28b-W172F plasmids; Lane 1 and 2, pET28b-W172F clone 1 and 2 digested with *Xho*I and *Nde*I.

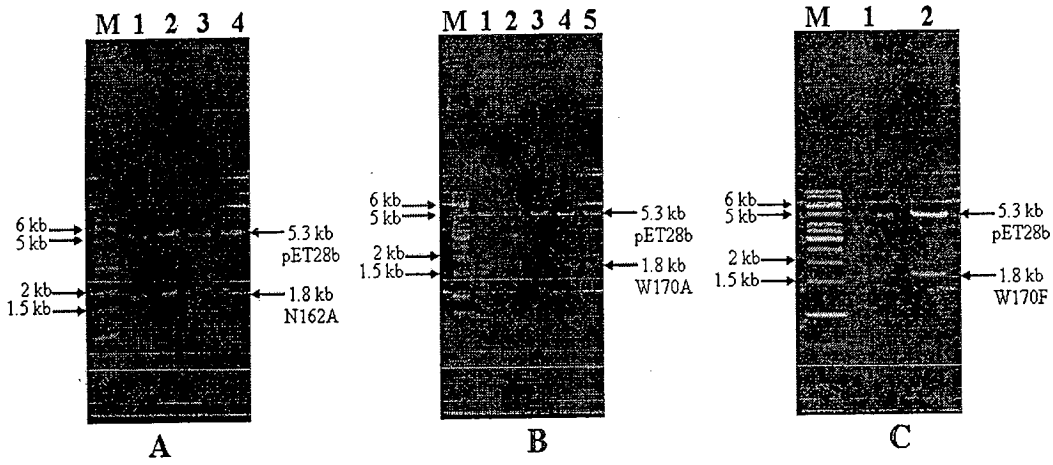

Figure 7 Restriction enzyme analysis of OsBADH2 mutants. (A) Restriction enzyme analysis of pET28b-N162A plasmids; Lane M, GeneRuler DNA Ladder; Lane 1-4, pET28b-N162A clone 1-4 digested with *Xho*I and *Nde*I; (B) Restriction enzyme analysis of pET28b-W170A plasmids; Lane 1-5, pET28b-W170A clone 1-5 digested with *Xho*I and *Nde*I; (C) Restriction enzyme analysis of pET28b-W170F plasmids; Lane 1 and 2, pET28b-W170F clone 1 and 2 digested with *Xho*I and *Nde*I.

DNA sequencing was used to confirm the mutation on the *OsBADH1* and *OsBADH2*. The sequencing result of N164A, W172A, N162A and W170A showed the codon GCT, GCG, GCC and GCG which codes for alanine, respectively. Likewise, the sequencing result of both W172F and W170F showed the codon TTC which codes for phenylalanine.

```
Wildtype_OsBADH1    ACTCCCTGGAATTATCCTCTGCTGATGGCTACTTGGAAGGTTGCACCTGCCCTGGCTGCT 540
N164A               ACTCCCTGGGCTTATCCTCTGCTGATGGCTACTTGGAAGGTTGCACCTGCCCTGGCTGCT 540
W172A               ACTCCCTGGAATTATCCTCTGCTGATGGCTACTGCGAAGGTTGCACCTGCCCTGGCTGCT 540
W172F               ACTCCCTGGAATTATCCTCTGCTGATGGCTACTTTCAAGGTTGCACCTGCCCTGGCTGCT 540
                    ********* ********************** ************************
```

Figure 8 Pairwise alignment of partial DNA sequencing of wild-type and mutant of OsBADH1 using ClustalW2. The mutation sites for the N164A, W172A and W172F are shown in bold and underlined.

```
Wildtype_OsBADH2    TGGAACTATCCTCTCCTGATGGCAACATGGAAGGTAGCTCCTGCCCTGGCTGCTGGCTGT 540
N162A               TGGGCCTATCCTCTCCTGATGGCAACATGGAAGGTAGCTCCTGCCCTGGCTGCTGGCTGT 540
W170A               TGGAACTATCCTCTCCTGATGGCAACAGCGAAGGTAGCTCCTGCCCTGGCTGCTGGCTGT 540
W170F               TGGAACTATCCTCTCCTGATGGCAACATTCAAGGTAGCTCCTGCCCTGGCTGCTGGCTGT 540
                    ***  ********************** ******************************
```

Figure 9 Pairwise alignment of partial DNA sequencing of wild-type and mutant of OsBADH2 using ClustalW2. The mutation sites for the N162A, W170A and W170F are shown in bold and underlined.

3.2. Protein expression and purification of OsBADH1 and OsBADH2

After the DNA sequence of the mutated *OsBADH1* and *OsBADH2* was confirmed, the chosen mutated plasmids were transformed into *E. coli* BL21 (DE3). All mutants were expressed and purified as described in methodology section. In small scale expression, cells were harvested before and after the induction with IPTG and then applied to 12% SDS-PAGE. It was found that the protein could be well expressed at 22 °C with the induction of 0.4 mM IPTG. Then the large scale expression of OsBADH1 and OsBADH2 was performed in 500 ml LB medium. The expected size of either OsBADH1 or OsBADH2 was 56 kDa and 58 kDa as shown in Figure 10 and Figure 11, respectively. The result indicated that OsBADH1 and OsBADH2 were vastly expressed as a soluble form but a few were expressed as an insoluble inclusion bodies. To purify the proteins, the harvested cells were lysed by extraction buffer and the soluble protein was centrifuged to separate the cell debris. The clarified supernatant was applied to HiTrap affinity column. The 6xHis proteins were eluted by an increasing imidazole gradient of elution buffer. The cell pellets, unbound and bound fractions from the purification were subjected to 12% SDS-PAGE as shown in Figure 12 and Figure 13. The result indicated that all OsBADH1 and OsBADH2 wild-type and mutants were purified to high yield and have an apparent molecular weight of 56 kDa and 58 kDa, respectively.

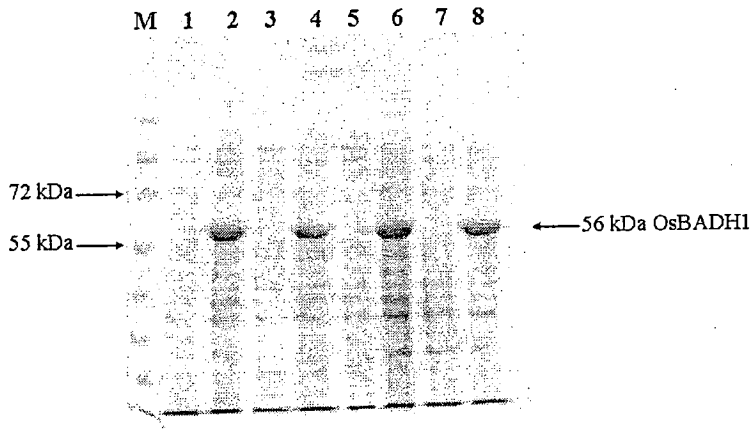

Figure 10 Expression analysis of OsBADH1 wild-type and mutants. Lane M, PageRuler prestained protein ladder; Lane 1-2, Expression of OsBADH1 wild-type protein for 0 hr and overnight; Lane 3-4, Expression of N164A protein for 0 hr and overnight; Lane 5-6, Expression of W172A protein for 0 hr and overnight; Lane 7-8, Expression of W172F protein for 0 hr and overnight.

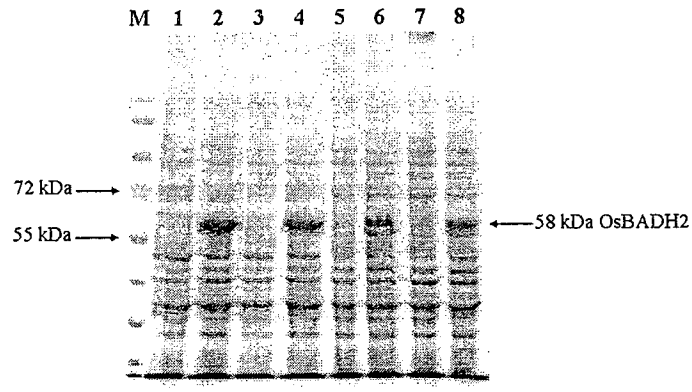

Figure 11 Expression analysis of OsBADH2 wild-type and mutants. Lane M, PageRuler prestained protein ladder; Lane 1-2, Expression of OsBADH2 wild-type protein for 0 hr and overnight; Lane 3-4, Expression of N162A protein for 0 hr and overnight; Lane 5-6, Expression of W170A protein for 0 hr and overnight; Lane 7-8, Expression of W170F protein for 0 hr and overnight.

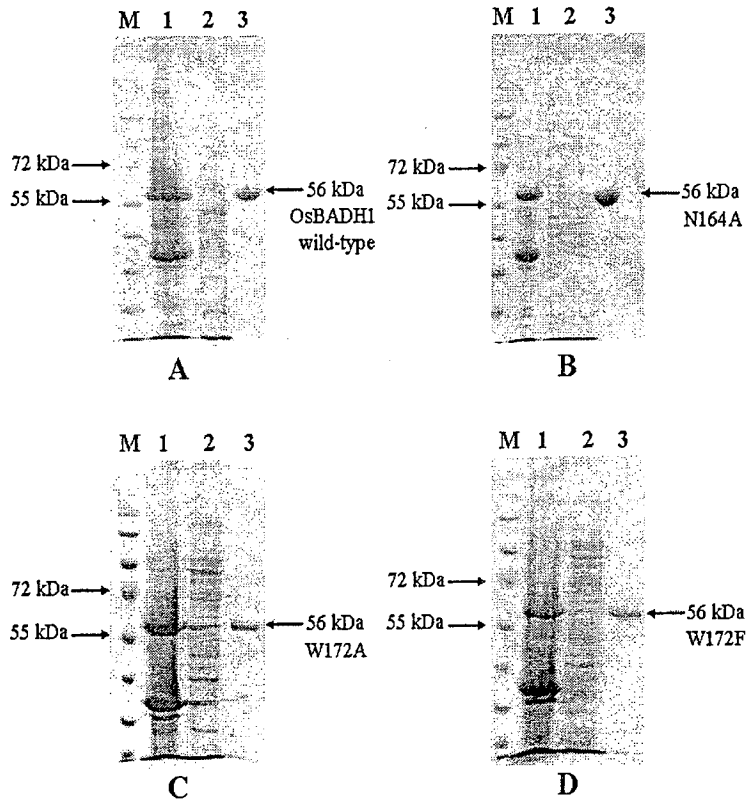

Figure 12 SDS-PAGE analysis of OsBADH1 purification. (A) Purification of OsBADH1 wild-type; (B) Purification of N164A; (C) Purification of W172A; (D) Purification of W172F; Lane M, PageRuler prestained protein ladder; Lane 1, insoluble fraction ; Lane 2, unbound fraction; Lane 3, the eluted protein.

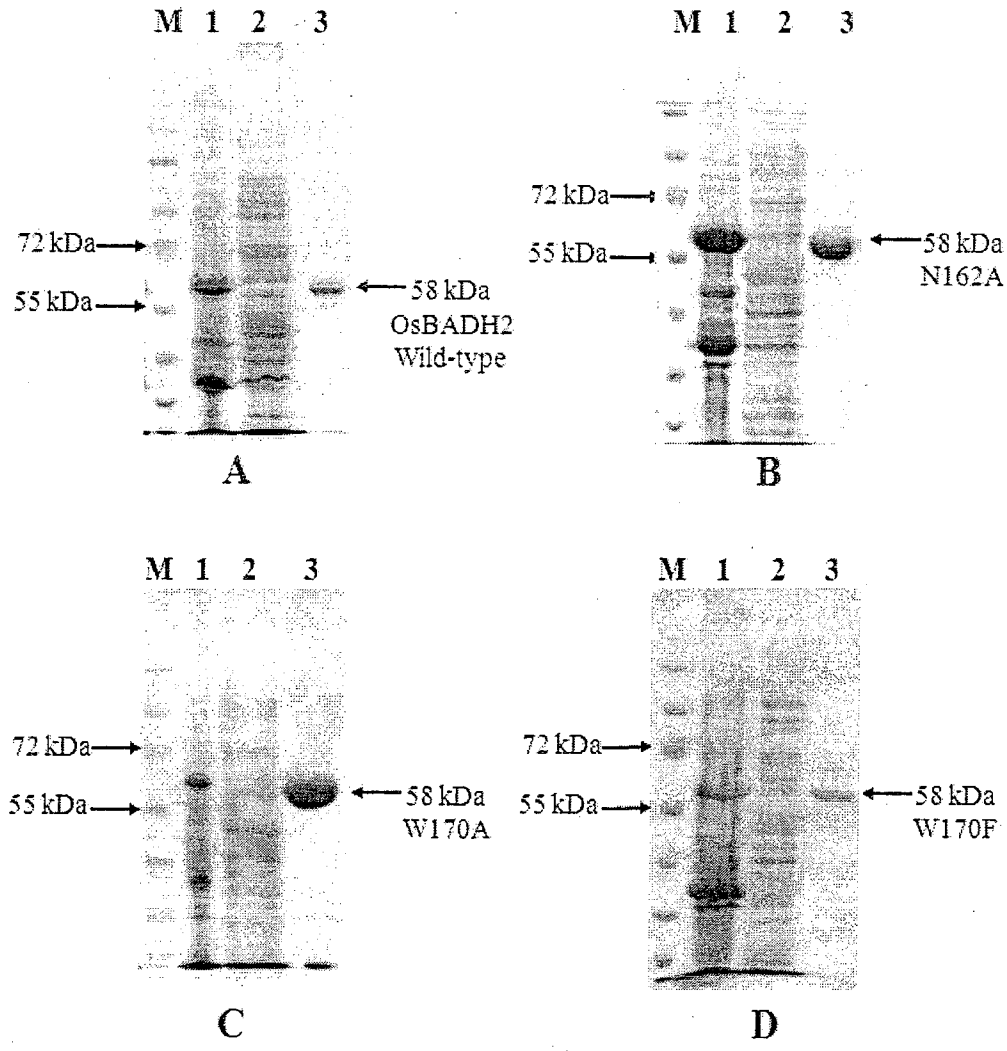

Figure 13 SDS-PAGE analysis of OsBADH2 purification. (A) Purification of OsBADH2 wild-type; (B) Purification of N162A; (C) Purification of W170A; (D) Purification of W170F; Lane M, PageRuler prestained protein ladder; Lane 1, insoluble fraction ; Lane 2, unbound fraction; Lane 3, the eluted protein.

3.3. NAD^+ binding study of OsBADH1 and OsBADH2

To investigate whether the mutation affected the overall folding of the protein, the NAD^+ binding study was carried out. The affinity between the enzymes and NAD^+ was investigated by the intrinsic tryptophan fluorescence study. The intrinsic tryptophan fluorescence of OsBADHs was recorded on the free enzyme and on the addition of NAD^+. The fluorescence properties of tryptophan amino acid residues can be altered upon co-factor binding. The conformation changes in the presence of ligand can result in fluorescence enhancement which can be examined protein-ligand interaction. Figure 14 and 45 reveals the modeled structure of OsBADH1 and OsBADH2 with tryptophan side chains and NAD^+, respectively.

Figure 14 The protein structure of OsBADH1. The structure of OsBADH1 is shown in ribbon (orange). The tryptophan side chains are shown in stick and colored by atoms (carbon, cyan). The ADP moiety of NAD^+ are depicted in sphere representation and colored by atoms (carbon, green slate).

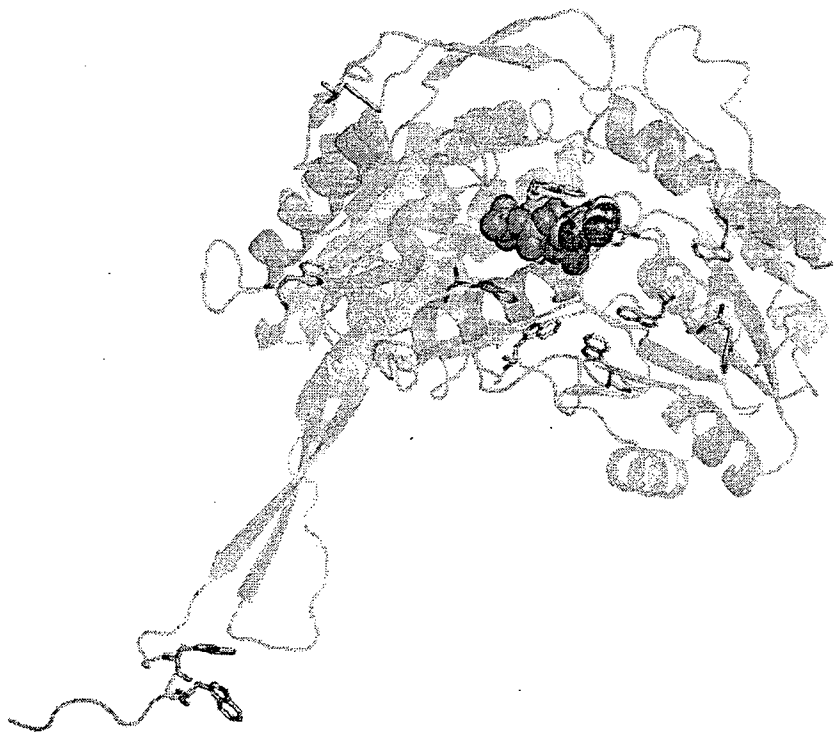

Figure 15 The protein structure of OsBADH2. The structure of OsBADH2 is shown in ribbon (magenta). The tryptophan side chains are shown in stick and colored by atoms (carbon, cyan). The ADP moiety of NAD^+ are depicted in sphere representation and colored by atoms (carbon, green slate).

From Figures 14-15, OsBADH1 contains 11 tryptophan residues including W18, W68, W163, W172, W283, W319, W392, W448, W461, W476 and W498 whereas OsBADH2 contains 13 tryptophan residues including W16, W66, W109, W161, W170, W281, W288, W317, W390, W446, W459, W494 and W496. The structure of OsBADH2 was obtained from Assist. Prof. Dr. Kiattawee Choowongkomon (Department of Biochemistry, Kasetsart University, Thailand) (Kuaprasert *et al.*, 2011) and that of OsBADH1 was gained from the homology modeling using OsBADH2 as a template. More details regarding the homology modeling are described in section 5 of this chapter. According to the crystal structure of OsBADH2, only the ADP moiety of the NAD^+ coenzyme is well defined in density. Several reports have previously shown that BADHs from several species can bind either NAD^+ or $NADP^+$ (Gruez *et al.*, 2004; Fujiwara *et al.*, 2008; Tylichová *et al.*, 2010; Wongpanya *et al.*, 2011). YdcW, a BADH from *E. coli*, has much better affinity for NAD^+ than for $NADP^+$ (Gruez *et al.*, 2004) while BADHs in barley, BBD1 and BBD2, can also bind NAD^+ better than $NADP^+$ (Fujiwara *et al.*, 2008). Likewise, BADHs in rice, OsBADH1 and OsBADH2, can also bind NAD^+ better than $NADP^+$ (Wongpanya *et al.*, 2011). According to BADHs in *Pisum sativum*, PsAMADH1 and PsAMADH2, were tested with several NAD^+ analogs (Tylichová *et al.*, 2010). The result shows that $NADP^+$ is a poor electron acceptor, reducing the activity of both enzymes by 85% comparing to

NAD^+. Using the purified recombinant OsBADHs, the affinity of the enzymes and NAD^+ was investigated using the intrinsic tryptophan fluorescence study. The intrinsic tryptophan fluorescence of OsBADHs was recorded on the free enzyme and on the addition of NAD^+ to determine the direct affinity of NAD^+ and enzymes. The fluorescence properties of tryptophan amino acid residues can be altered upon co-factor binding. The conformation changes in the presence of ligand can result in either fluorescence quenching or enhancement, which can examine protein-ligand interaction. For BADH proteins, it has been reported that the binding of NAD^+ usually takes place prior to the binding of aldehyde substrate (Perez-Miller *et al.*, 2003). When the wavelength at 295 nm was used to excite the tryptophan residues within the protein, the emission spectrum of OsBADHs exhibited a maximum wavelength at 350 nm. The decrease of the intensity of tryptophan fluorescence of OsBADHs can be observed upon the addition of NAD^+ (0–0.55 mM). This phenomenon is clearly associated to the binding of NAD^+, which can imply that the overall folding of the enzyme was correct and the mutations to the OsBADH active site do not induce considerable conformational changes. Since the same phenomenon was also observed in YdcW, a BADH from *E. coli* (Gruez *et al.*, 2004) and BADH2 from rice (Wongpanya *et al.*, 2011). The dissociation constant (K_d) values of OsBADH1 and OsBADH2 wild-type and mutants were determined for NAD^+ as shown in Table 16.

The K_d values of all mutants were increased less than 2-fold, indicating that the mutation did not cause a dramatic effect to the protein folding as well as the co-factor binding. The result of K_d values reported here is in agreement with the previously study (Wongpanya *et al.*, 2011). However, the K_d value of OsBADH2 for NAD^+ (9 μM) suggest that OsBADH2 can bind to NAD^+ with higher affinity compared to OsBADH1 (K_d of 34 μM). Collectively, the results showed that mutants could bind NAD^+, indicating the correct folding of the enzyme. The K_d values of BBD1 and BBD2 for NAD^+ (25.9 μM and 23.6 μM) have been reported (Fujiwara *et al.*, 2008) while the K_d values of PsAMADH1 and PsAMADH2 for NAD^+ were 40 μM and 55 μM, respectively (Tylichová *et al.*, 2010). Their K_d values were not largely different from the corresponding K_d values in this study. Having determined the co-factor binding affinity, the kinetic parameters K_m, k_{cat} and k_{cat}/K_m for OsBADHs wild-type and mutants were also characterized using Bet-ald and GAB-ald as substrates.

Table 6 Dissociation constant (K_d) of NAD^+ and OsBADHs

K_d (μM)			
OsBADH1		OsBADH2	
Wild-type	34 ± 3	Wild-type	9 ± 1
N164A	51 ± 3	N162A	19 ± 4
W172A	56 ± 3	W170A	16 ± 3
W172F	50 ± 3	W170F	14 ± 2

3.4. Enzymatic characterization of OsBADH1 and OsBADH2

Using the purified OsBADHs, Michaelis constants (K_m values), k_{cat} values and k_{cat}/K_m values for Bet-ald and GAB-ald can be obtained. All OsBADH1 and OsBADH2 wild-type and mutants can catalyze the oxidation of Bet-ald and GAB-ald as shown in Tables 7 8.

The K_m value of OsBADH1 wild-type for Bet-ald was 3-fold higher than GAB-ald, suggesting that OsBADH1 can bind GAB-ald better than Bet-ald. The K_m values of N164A, W172A and W172F for Bet-ald were observed with 7.8-fold, 10-fold and 9.2-fold decrease, respectively while K_m values of N164A, W172A and W172F for GAB-ald were 5.5-fold, 1.5-fold and 6.6-fold decrease, respectively in comparison to OsBADH1 wild-type. These results showed that all OsBADH1 mutants seemed to bind both Bet-ald and GAB-ald tighter than OsBADH1 wild-type did. Similarly to OsBADH1, K_m value of OsBADH2 wild-type for Bet-ald was 6.6-fold higher than GAB-ald while those of N162A, W170A and W170F for Bet-ald were observed with 3.8-fold, 3.3-fold and 4.4-fold decrease, respectively compared to OsBADH2 wild-type. In contrast, K_m values of N162A, W170A and W170F for GAB-ald were 2.8-fold, 1.5-fold and 2.8-fold increase, respectively compared to OsBADH2 wild-type. These results indicated that the mutants of OsBADH2 can bind Bet-ald tighter than wild-type but bind GAB-ald slightly less than wild-type. When comparing the K_m values of OsBADH1 and OsBADH2 for Bet-ald and GAB-ald to those previously reported (Bradbury *et al.*, 2008; Mitsuya *et al.*, 2009; Wongpanya *et al.*, 2011), our results are in comparable in that the enzymes can bind GAB-ald better than Bet-ald.

Table 7 Substrate specificities of OsBADH1 wild type and mutants

	OsBADH1					
	Bet-ald			GAB-ald		
	K_m (μM)	k_{cat} (s^{-1})	k_{cat}/K_m ($M^{-1} s^{-1}$)	K_m (μM)	k_{cat} (s^{-1})	k_{cat}/K_m ($M^{-1} s^{-1}$)
Wild-type	1288 ± 192	0.52	405	432 ± 57	0.31	718
N164A	165 ± 35	0.032	194	78 ± 5	0.023	295
W172A	129 ± 23	0.0022	17	291 ±18	0.22	756
W172F	140 ± 51	0.0102	73	65 ± 11	0.09	1385

Table 8 Substrate specificities of OsBADH2 wild type and mutants

	OsBADH2					
	Bet-ald			GAB-ald		
	K_m (μM)	k_{cat} (s^{-1})	k_{cat}/K_m ($M^{-1} s^{-1}$)	K_m (μM)	k_{cat} (s^{-1})	k_{cat}/K_m ($M^{-1} s^{-1}$)
Wild-type	251 ± 62	0.057	228	38 ± 11	0.032	842
N162A	66 ± 10	0.0093	141	107 ± 12	0.012	112
W170A	77 ± 7	0.0072	94	58 ± 8	0.01	172
W170F	57 ± 10	0.015	263	105 ± 10	0.14	1333

When the catalytic activity (k_{cat}) of the enzyme towards either Bet-ald or GAB-ald was investigated, the k_{cat} values of N164A, W172A and W172F for Bet-ald were found to be 16-fold, 236-fold and 51-fold decrease, respectively while those of N164A, W172A and W172F for GAB-ald were 13.5-fold, 1.4-fold and 3.4-fold decrease, respectively compared to OsBADH1 wild-type. For OsBADH2 variants, the k_{cat} values for Bet-ald of N162A and W170A had a 6-fold and 8-fold decrease, respectively, while the W170F mutant displayed a 3.8-fold increase in k_{cat} values for Bet-ald compared to wild type OsBADH2. Likewise, the k_{cat} values of N162A and W170A for GAB-ald were 2.7-fold and 3.2-fold smaller compared to the wild-type, respectively, but the W170F mutant had k_{cat} values 4.4-fold larger compared to that of the wild-type. Collectively, the results revealed that the alanine replacement of N164 and W172 of OsBADH1 and N162 and W170 of OsBADH2 studied in this paper reduced the catalytic activity towards Bet-ald and GAB-ald. However, W170F of OsBADH2 exhibited

slightly higher k_{cat} value for GAB-ald than the wild-type while W172F of OsBADH1 showed the reduced k_{cat} value.

In addition to the catalytic activity, the catalytic efficiency (k_{cat}/K_m) was also compared. For OsBADH1 mutants, the k_{cat}/K_m values of N164A, W172A and W172F for Bet-ald were reduced by 2.1-fold, 23.8-fold and 5.5-fold, respectively while those of N164A, W172A and W172F for GAB-ald decreased 2.4-fold, remained the same and increased 2-fold, respectively compared to OsBADH1 wild-type. For OsBADH2 mutants, the k_{cat}/K_m values of N162A, W170A and W170F for Bet-ald decreased 1.6-fold, decreased 2.4-fold and increased 1.2-fold, respectively while those of N162A, W170A and W170F for GAB-ald decreased 7.5-fold, decreased 4.9-fold and increased 1.6-fold, respectively. Out of six mutants, only two mutants (W172F of OsBADH1 and W170F of OsBADH2) showed a higher catalytic efficiency towards GAB-ald. This implied that either W172 or W170 in each protein may be a key residue for the substrate specificity towards GAB-ald. In addition to Bet-ald and GAB-ald, acetaldehyde was also used as a substrate since it was previously reported that both OsBADH1 and OsBADH2 catalyzed the oxidation of acetaldehyde (Table 19) (Mitsuya *et al.*, 2009). Accroding to Table 19, the result is in agreement with the previous report that with the higher k_{cat} and k_{cat}/K_m value, OsBADH1 is a better candidate enzyme for acetaldehyde than OsBADH2.

Table 9 Kinetic parameters of wild type OsBADHs with acetaldehyde

	Acetaldehyde		
	K_m (μM)	k_{cat} (s^{-1})	k_{cat}/K_m (M^{-1} s^{-1})
OsBADH1	99 ± 29	0.14	1425
OsBADH2	146 ± 34	0.08	607

BADH enzyme from *E. coli* was reported to be able to catalyze GAB-ald better than Bet-ald in general because of the shape of its active site (Gruez *et al.*, 2004). The size of the binding site is sufficient to accommodate molecules larger than Bet-ald such as n-alkyl medium chain aldehydes. Both Pea AMADH and OsBADHs also showed a broad substrate specificity utilizing various aminoaldehydes (C3-C6) as substrates (Šebela *et al.*, 2000; Tylichová *et al.*, 2010; Mitsuya *et al.*, 2009). It has also been reported that the residues C286, E252 and N153 make up the catalytic triad of the PaBADH active site in *Pseudomonas aeruginosa* (González-Segura1 *et al.*, 2009). In the active site, the hydroxyl oxygen of a bound glycerol molecule, which mimics the thiohemiacetal intermediate, is hydrogen bonded to the side chain of N153 and the main chain of C286 forming the oxyanion hole that stabilizes the intermediate (González-Segura *et al.*, 2009). In addition, the mutagenesis

of the highly conserved N162 of PsAMADH2 confirmed that the mutation of N162 to alanine resulted in about a 200-fold reduction in dehydrogenase activity, indicating that the residue is involved in the catalytic efficiency of PsAMADH2 (Tylichová *et al.*, 2010). Therefore, the mutation on the catalytic Asn residue would definitely affect k_{cat}/K_m value. Besides the catalytic triad, the Trp residues around the substrate binding pocket was proposed to be involved in the substrate binding pocket (Johansson *et al.*, 1998), and hence the mutation on the Trp residues should also affect k_{cat}/K_m value when Trp residue was mutated. From overall results, most of the mutants exhibited lower or equal catalytic efficiency towards Bet-ald, while some mutants showed an increased catalytic efficiency towards GAB-ald than the wild type did. Additionally, changing Trp to Phe had a tremendous effect on k_{cat}/K_m towards GAB-ald but not towards Bet-ald. According to the kinetic results, Trp may be one of the recognition residues for Bet-ald but not for GAB-ald. Our result is well correlated with the study of aromatic active-site residues in PsAMADH2 (Kopečný *et al.*, 2011) in that aromatic residues in the substrate cavity, such as W170, W288 and Y163 (PsAMADH2 numbering), are important for the overall geometry of the substrate channel allowing for the appropriate orientation of the substrate towards the catalytic C294. These residues are also essential for π-electron stacking interaction with an entering substrate. Alanine scanning of aromatic residues in the substrate channel resulted in a change in substrate specificity of PsAMADH2 (Kopečný *et al.*, 2011). Since the crystal structure of complex between protein and aldehyde substrate is hard to come by and no structure of OsBADH is available; therefore, to gain a better understanding of the substrate specificity, molecular docking and molecular dynamics simulation were carried out.

3.5. Molecular docking analysis of OsBADH1 and OsBADH2

In order to visualize the spatial arrangement of the substrate in the substrate binding pocket, molecular modeling of wild-type and mutants was carried out. To date, the crystal structure of BADH in rice has not been reported in PDB database. However, the condition to obtain the crystal of OsBADH in complex with NAD^+ was reported and the crystal structure of OsBADH2 was solved at 2.95 Å (Kuaprasert *et al.*, 2011) (unpublished data of Assist. Prof. Dr. Kiattawee Choowongkomon, Department of Biochemistry, Kasetsart University, Thailand). In order to validate this crystal structure, the comparison between the crystal structure and the modeled structure was carried out. Therefore, the crystal structure of OsBADH2 can be used as a template to create OsBADH1. The structure of OsBADH1 containing 498 residues (residues 8–504) was then modeled by SWISS-MODEL. The quality of the modeled OsBADH1 was evaluated using the program PROCHECK (Laskowski *et al.*, 1993). The model possesses good geometry, with 85% of all residues in the most favored and 14.6% in the allowed regions of the Ramachandran plot as indicated in Figure 16. The RMSD value between OsBADH1 and PsAMADH2 was 0.57 Å. Subsequently, the molecular docking of either

OsBADH1 or OsBADH2 wild-type and mutants was performed as described in methodology section.

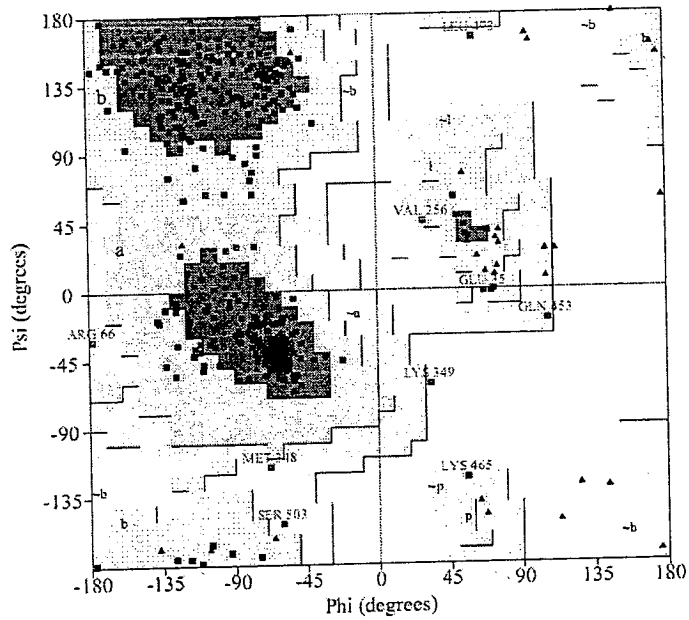

Figure 16. Ramachadran plot of OsBADH1 model. The red, yellow, cream and white regions represent the residues in most favored regions, additional allowed regions, generously allowed regions and disallowed regions, respectively.

To confirm the reliable of the result from molecular docking, the structure of OsBADH-substrate complexes from docking was superimposed with the structure of PsAMADH1 (PDB entry 3IWK) (Tylichová *et al.*, 2010) using PyMol (Delano, 2002). As can be seen in Figure 17, the position of both Bet-ald and GAB-ald overlaps well with a glycerol molecule in PsAMADH1, which is close to the catalytic cysteine and mimics a substrate bound to the substrate binding site. Moreover, the carbonyl aldehyde in both substrates is aligned closely to the catalytic cysteine. According to the binding energy, GAB-ald displayed the lowest binding energy of the OsBADH-substrate complexes than Bet-ald, indicating that GAB-ald is likely to bind both OsBADH1 and OsBADH2 with high affinity (Table 10).

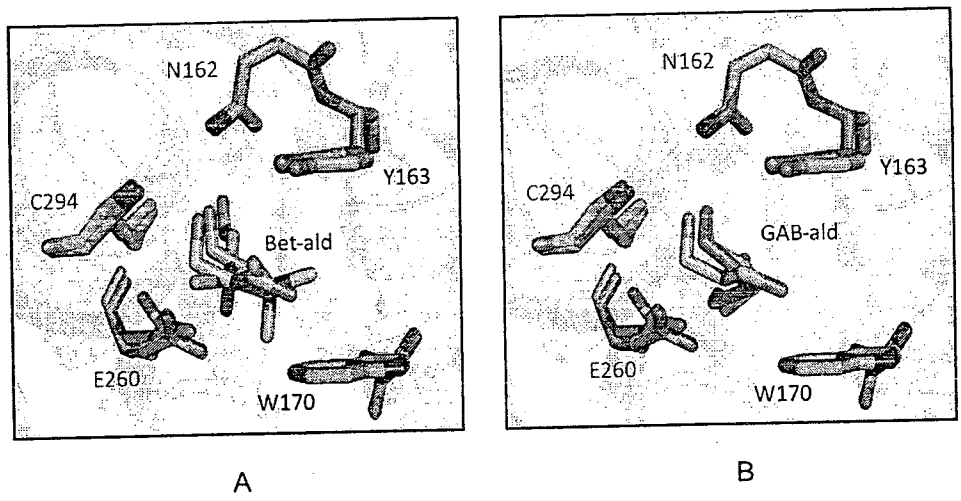

Figure 17. Superposition of OsBADH complexes from docking and PsAMADH1. (A) Superposition of PsAMADH1 and OsBADHs with Bet-ald (B) Superposition of PsAMADH1 and OsBADHs with GAB-ald. The amino acid residues of PsAMADH1 and glycerol are depicted in stick representation and colored by atoms (carbon, salmon). The color of OsBADH1-Bet-ald complex, OsBADH2-Bet-ald complex, OsBADH1-GAB-ald complex and OsBADH2-GAB-ald complex is shown in green, orange, cyan and magenta, respectively for carbon atoms. The red letter represents the catalytic triad residue of PsAMADH1 including C294, E260 and N162; the blue letter represents the aldehyde substrates whereas the black letter represents W170 and Y163 involved in the substrate recognition (*P. sativum* numbering).

Table 10 The lowest binding energy of wild-type and mutant OsBADHs from docking.

Binding energy (kcal/mol)					
	OsBADH1			OsBADH2	
	Bet-ald	GAB-ald		Bet-ald	GAB-ald
Wild-type	-3.66	-5.15	Wild-type	-4.03	-5.40
N164A	-3.78	-4.99	N162A	-4.07	-5.30
W172A	-3.68	-5.00	W170A	-3.83	-5.17
W172F	-3.81	-5.15	W170F	-4.00	-5.35

The binding pockets of OsBADH1 and OsBADH2 in complex with Bet-ald and GAB-ald are shown in Figure 5 and Figure 6 with the hydrogen bonding analysis. It can be seen that the carbonyl group of Bet-ald can form two moderate to strong hydrogen bonds between the N-H main chain of C296 and the N-H side chain of N164 in OsBADH1-Bet-ald complex (Figure 18A) with a distance of 1.9 Å for C296 and 2.3 Å for N164. In N164A-OsBADH1-Bet-ald complex, the hydrogen bond between the N-H side chain of N164 and the carbonyl group of Bet-ald was abolished when residue N164 was replaced with alanine (Figure 18B). In W172A and W172F-OsBADH1-Bet-ald complexes, two strong hydrogen bonds were also observed as the same manner as those in wild-type OsBADH1 (Figure 18C). However, the distances of

hydrogen bonds formed in all mutants were slightly longer than those observed wild-type. It is important to note that the tertiary amine group of Bet-ald was positioned away from the mutated residue whereas the oxygen was positioned toward the catalytic cysteine. Unlike OsBADH1-Bet-ald complex, four hydrogen bonds can be determined in wild-type OsBADH1-GAB-ald and W172A-OsBADH1-GAB-ald. Five hydrogen bonds are observed in W172F in complex with GAB-ald (Figure 18F). In OsBADH1 mutants – GAB-ald complex, the hydrogen bond between the N-H side chain of N164 and the carbonyl group of GAB-ald was also disturbed when residue N164 was changed to alanine (Figure 18E). Higher numbers of hydrogen bonds in GAB-ald complex collaborate well with the kinetic results in which the K_m values for GAB-ald are slightly lower than those for Bet-ald. It is also noted that the amino group in GAB-ald is pointed toward E262 instead of W172. This therefore revealed the difference in the substrate recognition of OsBADH1.

In comparison to the OsBADH1-Bet-ald complex, similar patterns of hydrogen bond network were observed in the OsBADH2-Bet-ald complex. The N-H main chain of C294 and the N-H side chain of N162 can form hydrogen bonds with the oxygen carbonyl group of Bet-ald as seen in the OsBADH1 complex (Figure 19A). Similar to OsBADH1, the N162A mutation caused the loss of hydrogen bond (Figure 19B) but the same pattern of hydrogen bonds is observed in the W170A and W170F complexes (Figure 19C). For the OsBADH2-GAB-ald complex, four hydrogen bonds can be found between GAB-ald and residues C294, N162 and E260 (Figure 19D). It is noteworthy that two hydrogen bonds between N-H of GAB-ald and the carboxyl group of E260 are only detected in the complex with GAB-ald. However, in N162A- GAB-ald complex, only hydrogen bonds between the side chain of E260 and Bet-ald are observed (Figure 19E). On the other hand, five hydrogen bonds are observed in both W170A-GAB-ald and W170F-GAB-ald complex (Figure 19F). To further study the binding mode of both Bet-ald and GAB-ald to wild-type OsBADHs as well as to determine the interactions involving in the protein–ligand complex, four complexes of the wild-type enzymes (OsBADH1-Bet-ald, OsBADH1-GAB-ald, OsBADH2-Bet-ald and OsBADH2-GAB-ald) obtained from the docking experiment were used for molecular dynamics (MD) simulations.

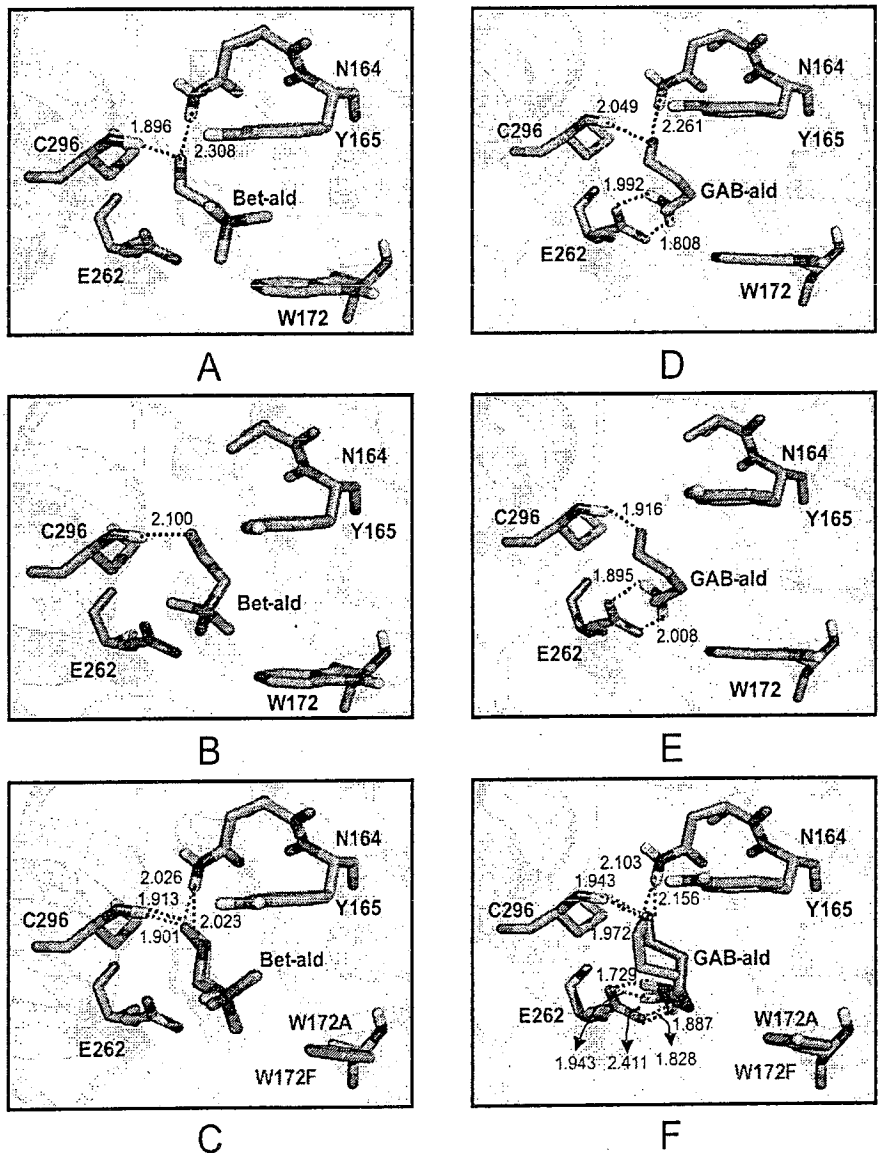

Figure 18 Molecular docking analysis of OsBADH1 complex. (A) the modeled OsBADH1 with Bet-ald (B) the modeled N164A with Bet-ald (C) the modeled W172A and W172F with Bet-ald (D) the modeled OsBADH1 with GAB-ald (E) the modeled N164A with GAB-ald (F) the modeled W172A and W172F with GAB-ald. The H-bonds are shown in dot line. The color of OsBADH1, N164A, W172A and W172F is shown in green, orange, cyan and magenta, respectively for carbon atoms. The red letter represents the catalytic triad residue of OsBADH1 including C296, E262 and N164. The green letter represents the aldehyde substrates, Bet-ald and GAB-ald. Distances are in angstrom.

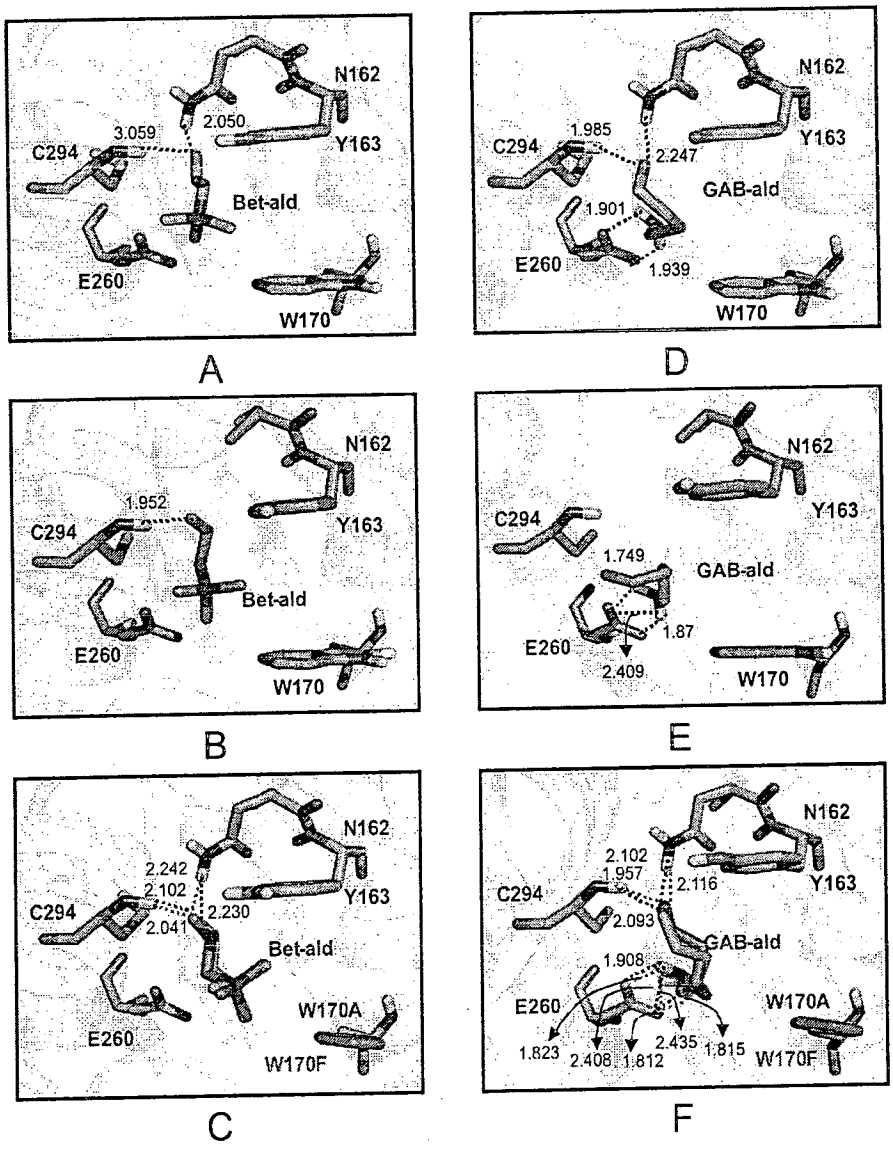

Figure 19 Molecular docking analysis of OsBADH2 complex. (A) the modeled OsBADH2 with Bet-ald (B) the modeled N162A with Bet-ald (C) the modeled W170A and W170F with Bet-ald (D) the modeled OsBADH2 with GAB-ald (E) the modeled N162A with GAB-ald (F) the modeled W170A and W170F with GAB-ald. The H-bond was shown in dot line. The color of OsBADH2, N162A, W170A and W170F is shown in green, orange, cyan and magenta, respectively for carbon atoms. The red letter represents the catalytic triad residue of OsBADH2 including C294, E260 and N162. The green letter represents the aldehyde substrates, Bet-ald and GAB-ald. Distances are in angstrom.

3.6. Molecular dynamics (MD) simulations of OsBADH1 and OsBADH2

According to MD simulation, the statistical analysis was applied to observe the equilibrium distance and hydrogen bonding interactions. Some atoms of the ligands and the receptors moved closer to or further from each other in equilibrium due to the dynamics in the binding process. The conformation of either Bet-ald or GAB-ald upon binding to both OsBADH complexes was examined (Figure 20). In OsBADH1-Bet-ald, only one hydrogen bond was observed (Figure 51A) between the main chain of C296 (N) and the oxygen atom (O) of Bet-ald with an average distance of 2.91 Å. In OsBADH1-GAB-ald, four hydrogen bonds observed are the following (Figure 51B): E262 (O) and GAB-ald (H1), GAB-ald (N1) and W454 (HE1), GAB-ald (O1) and C296 (H) and L263 (O) and GAB-ald (H2) with average distances of 2.88, 2.90, 2.89 and 2.89 Å, respectively. In OsBADH2, no hydrogen bonds were observed for Bet-ald (Figure 51C) but five hydrogen bonds were observed for GAB-ald (Figure 51D). The five hydrogen bonds in the OsBADH2-GAB-ald complex contained GAB-ald (O1) and C294 (H), L261 (O) and GAB-ald (H2), GAB-ald (O1) and N162 (HD21), GAB-ald (N1) and W456 (HE1) and E260 (O) and GAB-ald (H1) with average distances of 2.87, 2.89, 2.91, 2.92 and 2.91 Å, respectively. In the light of the MD simulation, it was revealed that GAB-ald formed stronger hydrogen bonds than Bet-ald with the OsBADH1. As for OsBADH2, five hydrogen bonds were formed in the OsBADH2-GAB-ald complex while none was observed in OsBADH2-Bet-ald complex. In addition to hydrogen bond formation, relationships between the orientation of the Bet-ald and GAB-ald in the complex were different. First, Bet-ald in OsBADH1 complex was far away from the catalytic triad compared with that in OsBADH2 complex. It is important to note that the position of Bet-ald observed in the crystal structure of BADH in *E. coli* was also different from that in PaBADH (Gruez *et al.*, 2004; González-Segura *et al.*, 2009). Secondly, when looking at the two substrates, GAB-ald was located closer to the catalytic residue, E262 compared to Bet-ald. This finding here was in agreement with the previous work, reporting that BADH catalyzes GAB-ald (C3-C6 aminoaldehydes) better than Bet-ald (Mitsuya *et al.*, 2009; Tylichová *et al.*, 2010).

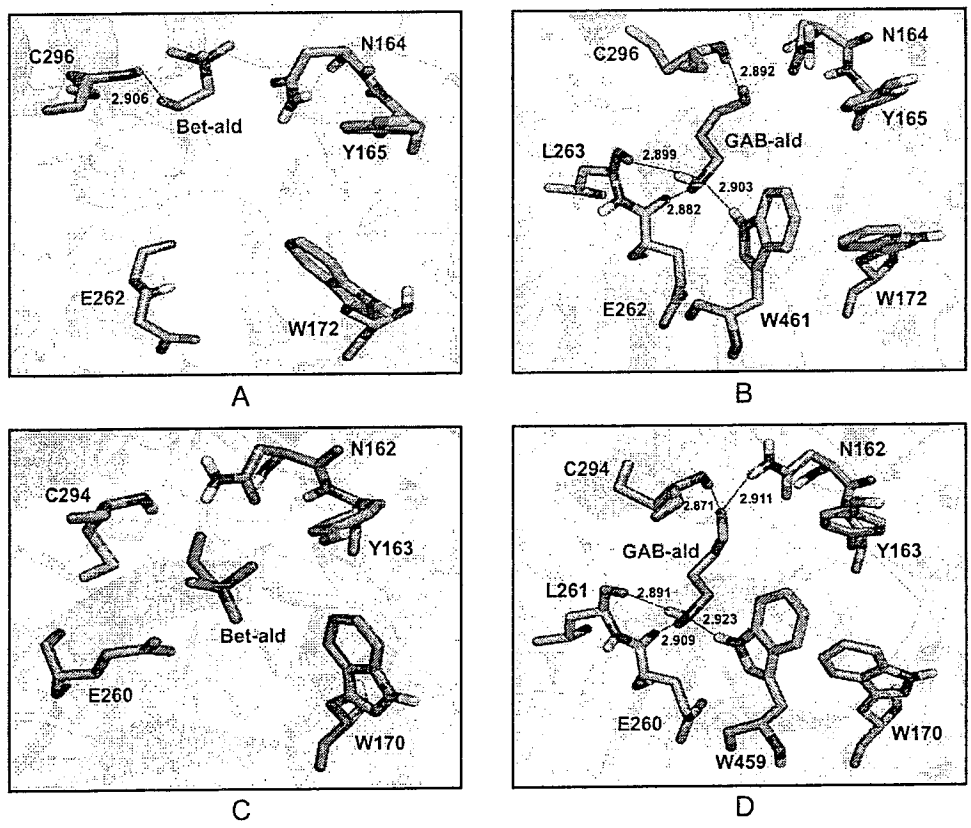

Figure 20 Active site of OsBADH-ligand complexes from MD simulations. (A) modeled OsBADH1 with Bet-ald (B) modeled OsBADH1 with GAB-ald (C) modeled OsBADH2 with Bet-ald (D) modeled OsBADH2 with GAB-ald. The hydrogen bonds are shown in dot line. The color of OsBADH1-Bet-ald, OsBADH1-GAB-ald, OsBADH2-Bet-ald and OsBADH2-GAB-ald is shown in green, cyan, orange and magenta, respectively for carbon atoms. The red letter represents the catalytic triad residues of OsBADH1 including C296, E262 and N164 whereas OsBADH2 including C294, E260 and N162. The pink letter represents the aldehyde substrates, Bet-ald and GAB-ald. Distances are in angstrom.

3.7. Conformation of the catalytic Cysteine and Glutamate

The conformation of catalytic Cys and Glu was observed from MD simulations of the OsBADH-ligand complexes. According to the previous study, the catalytic Cys residue can adopt two conformations: the "resting" conformation in which the Cys residue is far from the carbonyl carbon of the bound aldehyde (González-Segura *et al.*, 2009), and the "attacking" conformation in which the Cys residue is close to this carbon in the correct position to perform the nucleophilic attack. In the case of the catalytic Glu residue, three possible conformations have been observed: the "inside" conformation in which the Glu residue can activate the catalytic Cys residue for nucleophilic attack, since its carboxyl group is close to the thiol, the "intermediate" conformation in which the Glu residue is suited for the activation of the hydrolytic water molecule and the "outside" conformation in which the catalytic Glu releases the proton that was previously taken from either the catalytic Cys or a hydrolytic water involved in the proton relay mechanism. The conformations of both

catalytic residues from PaBADH (PDB codes 2WME) and ALDH2 (PDB codes 1O02) are shown in Figure 21.

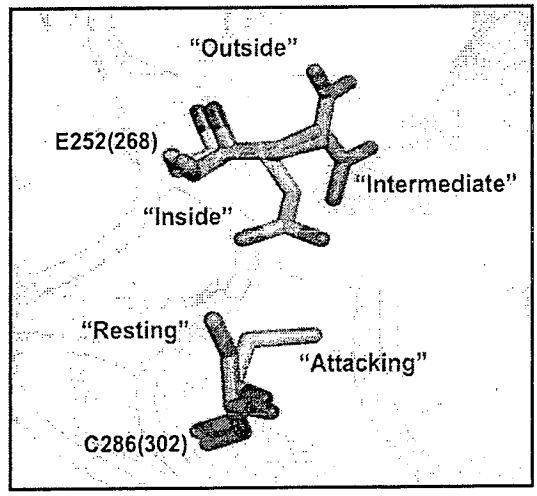

Figure 21 ALDH active sites. The distinct conformations of the catalytic Cys (resting and attacking) and catalytic Glu (inside, intermediate and outside) are displayed. The numbers of the residues correspond to PaBADH (2WME) and those within parenthesis to ALDH2 (1O02). Side chain atoms of residues are shown in stick and colored by atoms (PaBADH carbon: salmon pink, and ALDH2 carbon: lemon green).

The catalytic Cys (C286) in PaBADH is in the "resting" conformation and the catalytic Glu (E252) is found in both "outside" and "intermediate" conformations whereas in ALDH2 the catalytic Cys (C302) is found in the "attacking" conformation and the catalytic Glu (E268) is in "inside" conformation. When the structure of PaBADH is compared with the structure of ALDH2 and with OsBADH complexes from MD (Figure 22), it is revealed that the catalytic Glu residue in all structures exists in the "outside" conformation whereas the catalytic Cys residue is found in the "resting" conformation with the exception of the catalytic Glu residue of OsBADH2-Bet-ald complex that exists in an "inside" conformation. The negatively charged side chain of the catalytic Glu residue is positioned towards the positive quaternary ammonium of Bet-ald, suggesting it may have strong electrostatic interactions, consistent with the binding energy from MMGBSA decomposition. Additionally, the difference in the conformation of the catalytic Glu residue of OsBADH1 and OsBADH2 observed from MD simulations may also bring about the substrate specificity between the two substrates and the enzymes. Collectively, the work presented here for the first time provides the structure of OsBADH in complex with the substrates generated by MD. Further studies on other residues in the substrate binding pocket to better understand the substrate specificity are in progress.

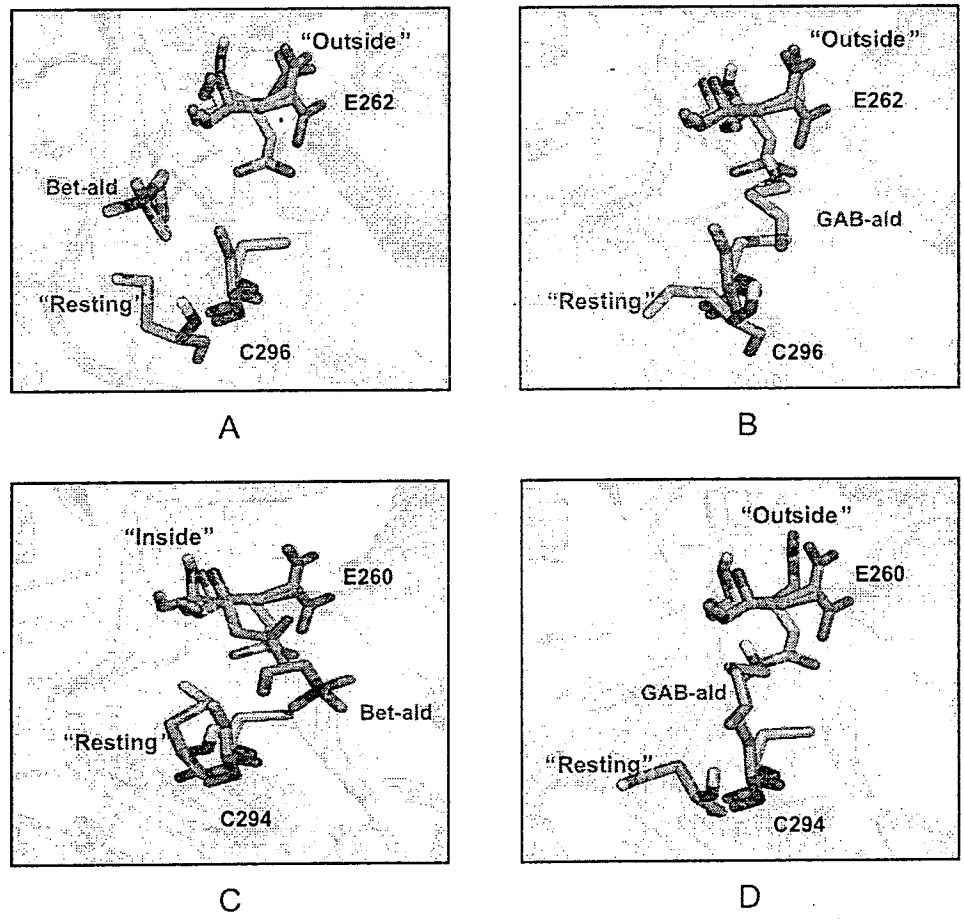

Figure 22 The conformations of active site residue in OsBADH-substrate complexes from MD simulations compared to PaBADH (2WME) and ALDH2 (1O02). (A) OsBADH1 with Bet-ald (B) OsBADH1 with GAB-ald (C) OsBADH2 with Bet-ald (D) OsBADH2 with GAB-ald. The black letter represents the catalytic residues of OsBADH1 including C296, E262 while OsBADH2 including C294, E260. The pink letter represents the aldehyde substrates, Bet-ald and GAB-ald. Side chain atoms of residue are shown in stick and colored by atoms (PaBADH carbon: salmon pink, ALDH2 carbon: lemon green, OsBADH1-Bet-ald carbon: green, OsBADH1-GAB-ald carbon: cyan, OsBADH2-Bet-ald carbon: orange, OsBADH2-GAB-ald carbon: magenta).